THE EFFECT OF HOT ISOSTATIC PRESSING ON STRUCTURAL AND MECHANICAL PROPERTIES OF METAL-BONDED DIAMOND GRINDING MATERIALS WITH HIGH POROSITY

[1]Jan JUŘICA, [1]Kateřina SKOTNICOVÁ, [1]Tomáš ČEGAN, [2]Filip JANHUBA, [2]Eduard MATÚS, [1]Jana RŮŽIČKA

[1]VSB - Technical University of Ostrava, Faculty of Materials Science and Technology, Ostrava, Czech Republic, EU, jan.jurica@vsb.cz

[2]Urdiamant s.r.o., Šumperk, Czech Republic, EU, filip.janhuba@urdiamant.com

https://doi.org/10.37904/metal.2024.4964

Abstract

This work deals with the increase in mechanical and utility properties of diamond grinding wheel with controlled porosity prepared by the sintering along the diamond grain boundary using binder material based on Cu-Sn-Ti alloy with subsequent hot isostatic pressing (HIP). The structure of diamond grinding wheel contained after sintering a large proportion of open porosity (35 to 39 %), which ensures a very good supply of coolant to the grinding point and at the same time removes the ground material from the grinding point. The effect of HIP on the structural characteristics, phase and chemical composition by SEM/EDX and XRD were studied in detail. The samples before and after HIP were subjected to the three-point bending test and the Vickers hardness test, which are the most important from the point of view of potential applications. The process of hot isostatic pressing led to the densification of necks formed between diamonds grains and to significant increase in the bending strength. The titanium-rich phases formed a shell around the diamond grains, improving their anchoring in the metal matrix. The grinding wheel showed very good utility properties that allow it to be used for long-term grinding with low resistance while maintaining shape stability during grinding.

Keywords: Hot isostatic pressing, mechanical properties, Cu-Sn-Ti alloy, diamond tools

1. INTRODUCTION

Because of its high hardness, chemical stability and wear resistance, diamond is widely used in the manufacture of tools to process the hard materials [1]. As the demand for efficiency in processing hard materials increases, the need for diamond tools with enhanced performance becomes crucial. This could involve improvements in cutting speed, precision, durability, and overall effectiveness in various industrial processes [2, 3]. Incorporating pore structure into diamond tool matrices allows for enhancing their performance in several ways. By introducing porosity, the chip capacity of the tool can be increased, allowing for more efficient removal of material during grinding processes. Additionally, these pores can serve as channels for cooling fluids, improving heat dissipation during operation. This cooling effect not only helps prevent overheating of the tool but also contributes to maintaining the integrity of the workpiece being processed. Moreover, the presence of pores can optimize the grinding function of diamond grits by providing space for debris generated during the machining process to evacuate, reducing the likelihood of clogging and enhancing the cutting efficiency of the tool. This, in turn, can lead to smoother surface finishes and improved dimensional accuracy of the workpiece. Overall, the integration of a pore structure within diamond tool matrices holds significant potential for optimizing the performance of diamond tools, ultimately resulting in enhanced productivity, longer tool life, and improved quality of machined components [4, 5]. However, it is important to note that pores fundamentally represent a kind of defects. So higher porosity could significantly impair the

strength of diamond tools [6, 7]. Extensive investigations into various methods of introducing pores into materials have been undertaken [8-10]. The use of pore-forming agents, such as TiH_2, has indeed emerged as a prominent technique for fabricating porous diamond tools with high porosity and strength. The advantage of this approach is its capability to customize the porosity of diamond tools while retaining sufficient mechanical strength for practical applications [11-13]. Fe-based and Cu-based alloy powders are commonly used as matrix materials for fabricating metal-based diamond tools. In comparison to Al alloy powders, Fe/Cu-based powders necessitate higher sintering temperatures, typically exceeding 800 °C. For example, the hot-pressing sintering temperatures of Fe-Co-Ni based [14] and Cu-Ni-Sn based [15] powders are approximately 950 °C and 850 °C, respectively. Liu et al. [16] added 7.5% of surface oxidation-treated TiH_2 powder to the Cu-Sn-Ti carcass powder and produced porous Cu-Sn-Ti based diamond tools with porosity of 15%.

This work deals with the effect of hot isostatic pressing (HIP) on structural and mechanical properties of diamond grinding materials with controlled porosity prepared by the sintering along the diamond grain boundary using binder material based on Cu-Sn-Ti alloy.

2. MATERIALS AND METHODS

The powders of copper(≥99.3 %), tin (≥99.5 %), titanium dihydride (≥99.5 %), Cu60Sn40 (wt%) and diamond grit were used as starting materials. The median diameter *D*50 of these powders is given in **Table 1**. The particle morphologies of Cu, Sn and TiH_2 powders are shown in **Figure 1**.

Table 1 The median diameter *D*50 of starting powders

Powder	Cu	Sn	TiH_2	Cu60Sn40	Diamond grit
***D*50** (μm)	5	20	100	125	D46

Two powder mixtures of grinding materials with the same composition were prepared using a Turbula mixer, one from pure powders (sample S1) and the other containing Cu60Sn40 pre-alloy (sample S2). The prepared mixtures were pressed with a pressure of 1 t/cm^2 using a hydraulic press. The compacts were sintered at a temperature of 880 °C for 20 minutes in a vacuum. To investigate the effect of HIP on structural characteristics and mechanical properties, the samples were subjected to hot isostatic pressing (HIP) at 630 °C for 40 minutes under a pressure of 100 MPa. Argon with a purity of 99.96 % was used during HIP.

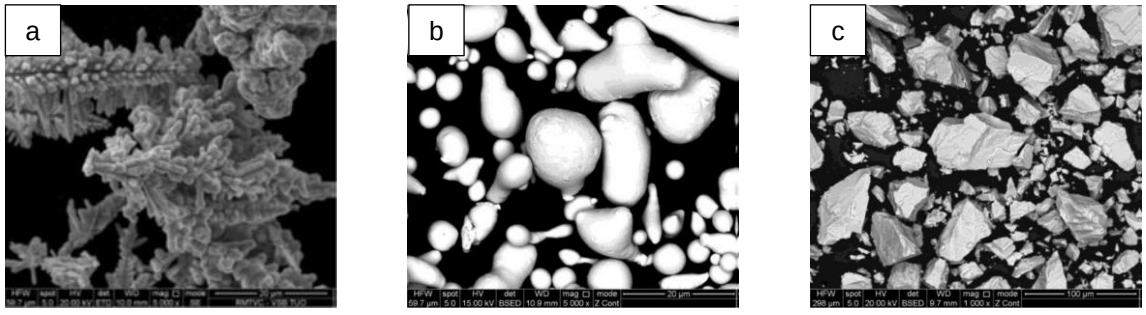

Figure 1 Back-scattered electron (BSE) micrographs of starting powders: a) Cu; b) Sn; c) TiH_2

The structural characteristics, chemical composition and distribution of alloying elements were investigated using a QUANTA 450 FEG scanning electron microscope (SEM) equipped with an energy dispersive X-ray EDX microprobe analysis. An INSTRON ElectroPuls E10 000 machine was utilized for the three-point bending test of samples before and after HIP. The hardness test was performed on equipment Future-tech FM-100 according to the Vickers method, namely HV0.1. Porosity and pore size distribution were measured using mercury porosimetry on an AutoPore IV 9500 instrument.

3. RESULTS AND DISCUSSION

The microstructure of samples S1 is documented in **Figure 2a** and **Figure 2b**, while the chemical composition of the detected phases is summarized in **Table 2** and **Table 3**. The SEM/EDX analysis of sample S1 before HIP process showed that its microstructure consisted of four main phases: Phase 1 corresponded to a matrix based on Cu-Sn with the Cu/Sn ratio of 3.8; Phase 2 corresponded Sn-Ti-Cu, contents of Ti and Cu are approximately the same; Phase 3 contained the most Ti, the content of Sn and Cu was almost the same (it is in the form of large dark grey areas in the structure); Phase 4 had a dominant Ti content and occurred at the diamond boundary.

The structure of sample S1 after the HIP process was characterized by the presence of four phases: Phase 1 corresponded to the Cu-Sn-based sample matrix with the Cu/Sn ratio of 3.8; Phase 2 was also based on Cu-Sn, but with a lower Sn content compared to the matrix (Cu/Sn ratio of 8.8), it was located between the grains of the matrix phase; Phase 3 was Ti-Cu-Sn based and occurred near the diamond boundary as both irregular particles and needles; Phase 4 was in the form of spheres and contained mostly Ti and Sn, with a minor amount of Cu.

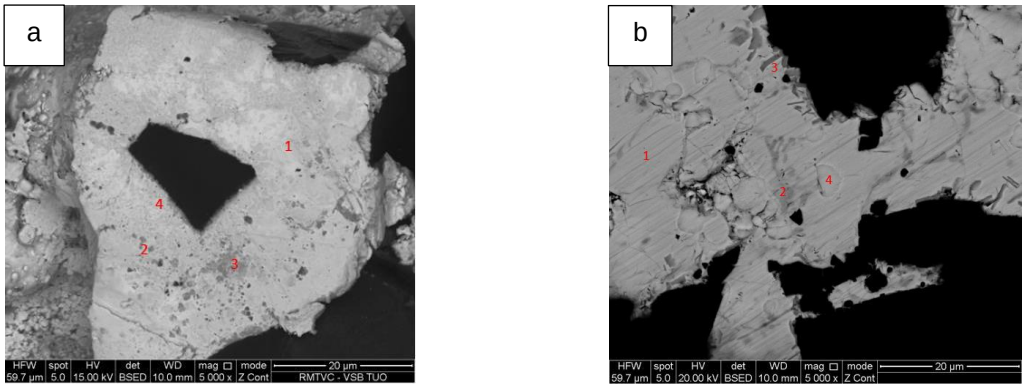

Figure 2 Microstructure of the sample S1 before (a) and after (b) the HIP process with marked EDX analysis spots

Table 2 Chemical composition of phases observed in the microstructure of sample S1 before HIP (in at%)

Phase/Element	Sn	Ti	Cu
Phase 1	20.9	0.5	78.6
Phase 2	42.4	28.0	25.8
Phase 3	23.8	38.2	22.0
Phase 4	22.3	55.3	7.7

Table 3 Chemical composition of phases observed in the microstructure of sample S1 after HIP (in at%)

Phase/Element	Sn	Ti	Cu
Phase 1	20.9	0.1	79.1
Phase 2	10.2	0.1	89.7
Phase 3	25.0	44.1	30.9
Phase 4	34.7	49.4	15.9

As can be seen from the X-ray maps of the distribution of alloying elements in the samples (**Figure 3** and **Figure 4**), the HIP process led to a significant change in the distribution of titanium. Its occurrence near the boundaries with diamond and

the formation of Ti-Sn and Ti-Sn-Cu based phases were observed.

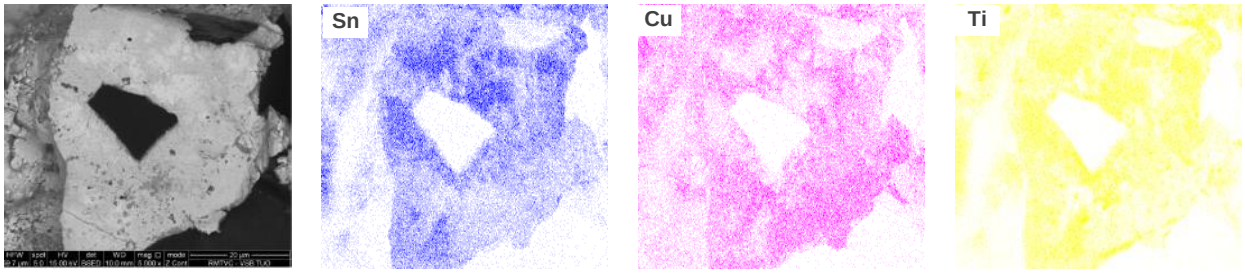

Figure 3 X-ray elemental distribution map of alloying elements in the sample S1 before HIP

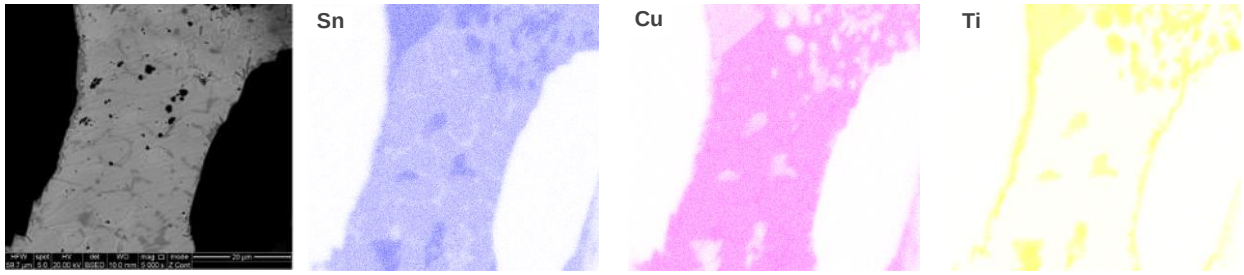

Figure 4 X-ray elemental distribution map of alloying elements in the sample S1 after HIP

The microstructure of samples S2 before and after HIP is documented in **Figure 5a** and **Figure 5b**, the chemical composition of the detected phases is summarized in **Table 4** and **Table 5**. The structure of sample S2 before the HIP process consisted of four phases: Phase 1 corresponded to sample matrix based on Cu-Sn with the Cu/Sn ratio of 3.6. Chemical analysis also showed significant inhomogeneity of the matrix; Phase 2 was based on Cu-Sn-Ti with the Cu/Sn ratio of 1.7 and formed small dark grey bounded areas; Phase 3 was a Sn-Ti-Cu-based phase that formed large dark gray areas; Phase 4 mainly contained Ti and occurred near the diamond boundaries in the form of elongated particles.

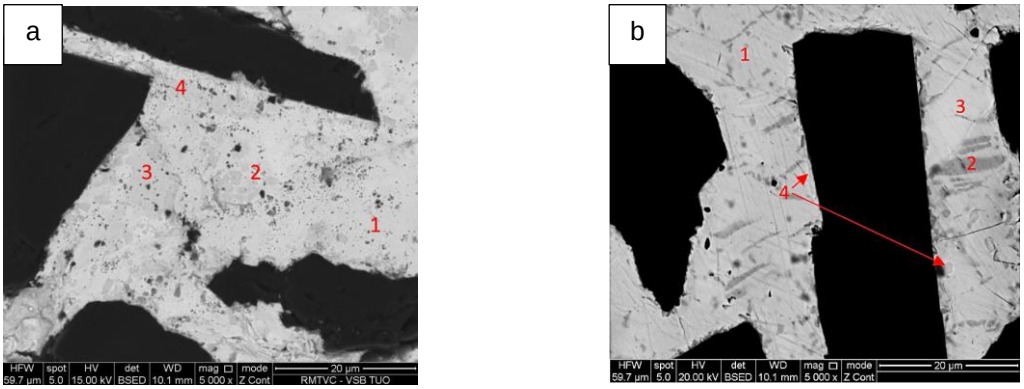

Figure 5 Microstructure of the sample S2 before (a) and after (b) the HIP process with marked EDX analysis spots

The structure of the S2 sample after the HIP process also contained four phases: Phase 1 corresponded to a Cu-Sn-based sample matrix with the Cu/Sn ratio of 3.7; Phase 2 was a Cu-rich phase with the Cu/Sn ratio of 9.2, located between grains of the matrix phase; Phase 3 with an elongated shape located near the diamond was Ti-Cu-Sn based; Phase 4 was also Ti-Sn-Cu based, but with higher Sn content and lower Cu content

compared to Phase 3. It was characterized by a rounded and elongated shape and location exclusively at diamond grain boundaries.

Table 4 Chemical composition of phases observed in the microstructure of sample S2 before HIP (in at%)

Phase/Element	Sn	Ti	Cu
Phase 1	21.6	0.5	77.9
Phase 2	31.2	12.8	54.2
Phase 3	39.0	34.4	21.8
Phase 4	5.8	57.6	20.3

Table 5 Chemical composition of phases observed in the microstructure of sample S2 after HIP (in at%)

Phase/Element	Sn	Ti	Cu
Phase 1	21.0	0.2	78.7
Phase 2	9.8	0.0	90.2
Phase 3	23.3	40.6	36.1
Phase 4	33.4	47.1	19.6

As can be seen from the X-ray maps of the distribution of alloying elements in the samples (**Figure 6** and **Figure 7**), there is a more homogeneous distribution of Cu and Sn. The Ti-enriched layer can again be observed near the grain boundaries of the diamond.

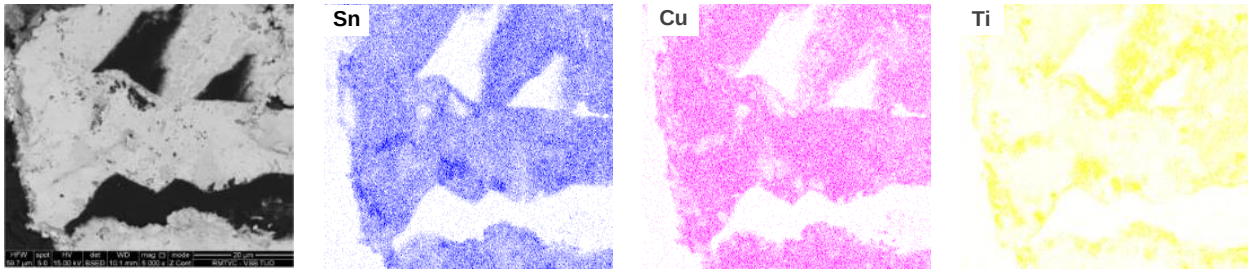

Figure 6 X-ray elemental distribution map and metallography of the initial sample S2 before HIP

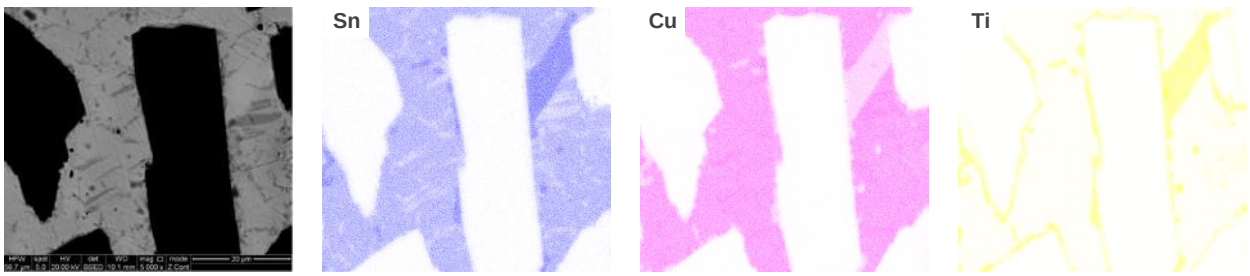

Figure 7 X-ray elemental distribution map and metallography of the initial sample S2 after HIP

The average value of the open porosity of the samples before HIP ranged from 36 to 39%. After the HIP process, the porosity value ranged from 34 to 38% - see **Table 6.**

It was found that the HIP process resulted in a threefold increase in flexural strength for samples – see **Table 6**. The HIP process led to the elimination of residual porosity in the region of the necks between the diamond

grains and thus to their densification. The Ti-Sn-Cu-based phase was modified, which initially had the shape of spherical particles, while after the HIP process it was in the form of needles. These effects led to an increase in mechanical properties. **Table 6** summarizes the determined values of hardness HV0.1 and bending strength.

Table 6 The values of bending strength, Vickers hardness HV0.1 and open porosity of samples

Sample	σ_{max} (MPa)	**HV0.1**	**Open porosity** (%)
S1 before HIP	75.1	569.6	39.08
S2 before HIP	63.2	524.8	35.64
S1 after HIP	206.1	591.2	37.85
S2 after HIP	206.1	565.0	34.02

4. CONCLUSIONS

Diamond grinding materials based on Cu-Sn-Ti matrix were prepared to investigate the effect of HIP on structural characteristics and mechanical properties. The following conclusions were reached:

- There was a high proportion of spherical particles of the titanium-based intermetallic phase at the diamond-matrix interface in Sample 1, which improved the anchoring of the diamonds in the matrix. This sample was prepared from pure powdered metals.
- Sample S2 contained a small proportion of spherical particles of a titanium-based intermetallic compound and was characterized by higher chemical homogeneity. Sample S2 was prepared from a Cu-Sn-based pre-alloy.
- After the HIP process, the Ti-rich phase was located around the diamond grains, resulting in strengthening necks between the diamond grains. Residual porosity in these areas was also eliminated.
- It can be concluded that the HIP process is an effective technology for increasing the mechanical properties of grinding materials with high porosity, as there was a significant increase in bending strength and hardness.

ACKNOWLEDGEMENTS

This study was carried out within the project TN02000018 National Centre of Competence ENGINEERING.

REFERENCES

[1] BING, C., WEIXING, Z., RUZHONG, Z., YAFANG, C., SUJUAN, Z., HAILING, L., WEIHUO, L., YUCAN, F., DONG, X. The abrasion resistance of brazed diamond using Cu–Sn–Ti composite alloys reinforced with boron carbide. *Diamond and Related Materials*. 2022, vol. 124. https://doi.org/10.1016/j.diamond.2022.108926.

[2] ZHOU, K., XU, J., XIAO, G, HUANG, Y. A novel low-damage and low-abrasive wear processing method of C f/SiC ceramic matrix composites: laser-induced ablation-assisted grinding. *Journal of Materials Processing Technology*. 2022, vol. 302. https://doi.org/ 10.1016/j.jmatprotec.2022.117503.

[3] DENKENA, B., GROVE, T., GOTTSCHING, T. Grinding with patterned grinding wheels. *CIRP Journal of Manufacturing Science and Technology*. 2015, vol. 8, p. 12–21. https://doi.org/10.1016/j.cirpj.2014.10.005.

[4] DENG, H., XU, Z. Dressing methods of superabrasive grinding wheels: a review. *Journal of Manufacturing Processes*. 2019, vol. 45, p. 46–69. https://doi.org/10.1016/j.jmapro.2019.06.020.

[5] SHU, G., CHUANG, K., LIAO, M., HUUANG, C., WU, M. Sintering, microstructure, and mechanical properties of vitrified bond diamond composite. *Ceramics International*. 2021, vol. 47, p. 33259–33268. https://doi.org/10.1016/j.ceramint.2021.08.227.

[6] DAVIS, TD., DICORLETO, J., SHELDON, D., VECCHIARELLI, J., ERKEY, C. A route to highly porous grinding wheels by selective extraction of pore inducers with dense carbon dioxide. *The Journal of Supercritical Fluids*. 2004, vol. 30, p. 349–358. https://doi.org/10.1016/j.supflu.2003.09.011.

[7] PENG, Y., REN, J., JIA, C., ZHONG, G., MA, Q., ZHANG, W. Structural design and mechanical properties of porous structured diamond abrasive tool by selective laser melting. *Ceramics International*. 2023, vol. 49, p. 6508–6521. https://doi.org/10.1016/j. ceramint.2022.10.136.

[8] DU, Z., ZHANG, F., XU, Q., HUANG, Y., LI, M., HUANG, H. Selective laser sintering and grinding performance of resin bond diamond grinding wheels with arrayed internal cooling holes. *Ceramics International*. 2019, vol. 45, p. 20873–20881. https://doi.org/10.1016/j. ceramint.2019.07.076.

[9] TOMINO, H., TSUKUDA, A., KONDO, Y., ISHIZAKI, K. Influence of porosity on grinding performance of porous cast-iron bonded diamond grinding wheel made by pulse electric current sintering method. *Journal of the Japan Society of Powder and Powder Metallurgy*. 1999, vol. 46, p. 257–261. https://doi.org/10.2497/jjspm.46.257.

[10] WU, Y., YAN, Q., ZHANG, X. Wear behavior of metal bond diamond composite with hollow spherical silica particles as pore former. *The International Journal of Advanced Manufacturing Technology*. 2019, vol. 104, p. 4757–4767. https://doi.org/10.1007/s00170-019-04364-z.

[11] HOU, S., ZHANG, S., WU, J. Effect of nickel-plated graphite on microstructure and properties of matrix for Fe-based diamond tools. *Transactions of Nonferrous Metals Society of China*. 2022, vol. 32, p.1575–88. https://doi.org/10.1016/S1003-6326(22)65894-1.

[12] LI, Y., LIU, X., ZHENG, J. A dual-ratiometric electrochemical sensor based on Cu/N doped porous carbon derived from Cu-metal organic framework for acetaminophen determination. *Microchemical Journal*. 2023, vol. 189. https://doi.org/10.1016/j. microc.2023.108556.

[13] MIAO, W., DING, Y., ZHAO, Y., BAO, H., YAN, N., YANG, W. Modified gel casting technique to fabricate honeycomb structured vitrified-bonded ultrafine diamond grinding wheels. *Ceramics International*. 2020, vol. 46, p. 4462–4469. https://doi.org/10.1016/j. ceramint.2019.10.172.

[14] KENNEDY, A.R. The effect of TiH_2 heat treatment on gas release and foaming in Al–TiH_2 preforms. *Scripta Materialia*. 2002, vol. 47, p. 763–767. https://doi.org/10.1016/S1359- 6462(02)00281-6.

[15] LOGINOV, P.A., SIDORENKO, D.A., SHVYNDINA, N.V., SVIRIDOVA, T.A., CHURYUMOV, A.Y., LEVASHOV, E.A. Effect of Ti and TiH_2 doping on mechanical and adhesive properties of Fe-Co-Ni binder to diamond in cutting tools. *International Journal of Refractory Metals and Hard Materials*. 2019, vol. 79, p. 69–78. https://doi.org/10.1016/j.ijrmhm.2018.11.008.

[16] CHEN, F., YAN, Z., LIU, Z., LONG, Y., FU, N., ZHANG, F., Preparation and properties of Al_2O_3-reinforced Cu-Ni-Sn metallic matrix for applications in diamond-cutting tools. *Diamond and Related Materials*. 2020, vol. 109. https://doi.org/10.1016/j. diamond.2020.108025.